Geometry effect on mechanical properties and elastic isotropy optimization of bamboo-inspired lattice structures

Miao Zhao [a,b], Xinwei Li [a], David Z. Zhang [c], Wei Zhai [a,*]

a Department of Mechanical Engineering, National University of Singapore, 117411, Singapore

b Chongqing Key Laboratory of Metal Additive Manufacturing (3D Printing), Chongqing University, Chongqing 400044, China

c College of Engineering, Mathematics and Physical Sciences, University of Exeter, North Park Road, EX4 4QF, UK

*Corresponding authors. E-mail address: mpezwei@nus.edu.sg

Abstract

Inspired by the geometry of bamboo, this study proposes a novel bamboo-inspired body-centered cubic (B-BCC) lattice structure consisting of tapered and hollow struts. Using representative volume elements applied with periodic boundary conditions, the mechanical properties and deformation behaviors of the B-BCC lattice structures are thoroughly evaluated by considering a large number of combinations of geometric parameters and volume fractions. Results reveal that the geometric parameters highly influence the deformation behavior of the B-BCC lattice structures under uniaxial compression (e.g, from bending- to stretching-dominated) but little under shear load. For this reason, tunable elastic modulus across a broad range can be realized via adjusting the geometric parameters and elastic isotropy can be obtained across all volume fractions. On this basis, a combination of artificial neural network and elastic isotropy optimization is proposed to obtain the isotropic B-BCC lattice structures with superior elastic modulus. The optimization results show that the elastic modulus of the isotropic B-BCC lattice structures increased by 271.24%-1335% and 17.72%-43.63%, as compared to the original BCC and isotropic hollow BCC lattice structures, respectively. Finally, the multi-layer simulation and compression experiments are applied to validate the optimization results. Good agreements are observed comparing the numerical and experimental results, demonstrating the effectiveness of the proposed bamboo-inspired design and optimization method for lightweight applications with desired properties.

Keywords: Bio-inspiration, Lattice structures, Mechanical properties, Structural optimization, Additive manufacturing

1. Introduction

Lattice structures are defined to be periodic cellular solids that consist of unit cells made up of three-dimensionally spatially architectured features [1]. For its unique architecture, lattice structures display unprecedented material properties. For their low density, lattice structures find applications as lightweight structural materials [2]. For their unique plateau deformation under compression, they also display excellent energy absorption properties [3, 4]. For their unique flow properties, they also function as sound absorbers [5] and thermal exchangers [6]. With the advent of additive manufacturing (AM), the fabrication of complex and custom-designed lattice structures with high

performances for the associated design requirements are made feasible [7-9].

The mechanical response of lattice structures can be classified into two primary categories: stretching-dominated and bending-dominated [10, 11]. Under a load, a stretching-dominated structure undergoes tension and compression of the struts, while a bending-dominated structure experiences the bending of the struts. Therefore, stretch-dominated structures usually have a high stiffness-to-weight ratio, while bending-dominated structures display excellent energy absorption characteristics [12]. The body-centered cubic (BCC) lattice structure is a typical bending-dominated lattice structure that has been wildly investigated in previous literature. For example, Gümrük et al. [13, 14] studied the static mechanical responses of BCC lattice structures under different loading conditions and established the theoretical equations to predict their physical and mechanical properties. Yang et al. [15] investigated the mechanical and fatigue performances of BCC lattice structures and proposed a stress concentration assessment method to evaluate fatigue performance. Mines et al. [16] conducted the compression and the drop weight impact experiments on BCC lattice structures and found a favorable impact performance of BCC lattice structures compared to honeycomb structures. In addition, the effects of volume fraction [17], unit cell size [18, 19], strut diameter [18], and unit cell pose [20] on the mechanical properties and deformation behavior were also numerically and experimentally investigated.

It should be noted that high stress concentrations are localized at the nodal regions of the BCC lattice structure owing to the bending of the struts [21]. This thus leads to poor mechanical properties, e.g., stiffness and strength, observed under the compression load. Therefore, many attempts have been made to optimize and improve the mechanical properties of BCC lattice structures. For example, fillets have been added to the nodal regions of BCC lattice structures to reduce stress concentration, and a 55% increase in stiffness is realized [22]. Similarly, nodal enforcements were also realized by adding spherical nodes [23] or smoothing the nodal regions by using minimal surfaces [24]. Furthermore, changing the shape of struts for the BCC lattice structure is another effective approach to improve the mechanical properties. The uniform struts of the BCC lattice structures were replaced by the ones with variable cross-sections, and the static and dynamic compression properties were increased due to the uniform stress distribution on tapered struts [21, 25-27]. Moreover, the design approach of BCC lattice structures with curved struts was also proposed, and the compression tests demonstrated that the curved design reduced the stress concentration and improved the load-bearing capacity [28]. The elastic modulus and compressive strength of BCC lattice structures also can be enhanced by adjusting the three-dimensional posture and mirror arrays of unit cells [29]. In addition to the change in the geometry of the BCC lattice structure, the mechanical enhancement was also realized by adding the reinforcing component [30-32]. For instance, Smith et al. [30] added a vertical strut to the BCC unit cell and designed the BCC-Z lattice structure. The added struts changed the deformation behavior from bending- to stretching-dominated and significantly enhanced the stiffness and strength [33]. Chapkin et al. [31] manufactured the composite BCC lattice structure by filling metallic BCC lattice structures with compressible foam. The compression tests demonstrated that the foam-infilled structure improved the volumetric energy dissipation and energy absorption efficiency by 19% and 12% compared to the unfilled one, respectively.

Through evolution and natural selection, biological structures found in nature have realized excellent physical and mechanical properties. Therefore, in addition to the aforementioned enforcement approaches, mimicking the biological structure in nature provides an innovative

alternative to the design of lattice structures with combined excellent mechanical properties and low density [34, 35]. Many researchers have recently leveraged the design concepts in nature and have worked on various novel lattice structures. For example, Pham et al. [36, 37] proposed damage-tolerant lattice structures inspired by the hardening mechanisms of crystal microstructure. The results showed that the crystal-inspired approach controlled the shear-band propagation and enhanced the mechanical properties and damage tolerance. Kumar et al. [38] studied a closed lattice structure inspired by the sea urchin and found the bio-inspired lattice structure improved the stiffness by 25% compared to open-cell lattice structures. Yang et al. [39, 40] designed a bi-directionally corrugated panel inspired by the telson of mantis shrimp and further investigated the geometric effects on static and dynamic mechanical properties through experiments and simulations. Additionally, inspired by the multiscale configuration of the microstructure of cork [41] and bone [42], the multilayered lattice structures composed of soft and hard materials were designed to enhance the toughness, shape recoverability, and energy absorption performance. It should be noted that bamboo is one particular biological organism that displays an excellent combination of high strength and light weight [43]. For instance, despite having a very high aspect ratio, it is capable of withstanding high bending stresses under the force exerted by the wind [34]. The excellent mechanical properties of bamboo derive from its hollow and tapered structure [44]. The hollow structure increases the moment of inertia of struts and minimizes the bending stress. The tapered structure effectively reduces the stress increase by shifting the position of maximum bending stress generation toward the part with a thicker diameter. Thus far, researchers have worked on introducing the bamboo structure to improve the axial and lateral energy absorption performance of thin-walled tubes [45, 46]. Moreover, the bamboo-inspired lattice structure with hollow struts was also designed [47], and the anisotropy properties can be tailored by tuning the outer and inner diameters of hollow struts [47-49].

Most of the previous studies focused solely on mimicking the hollow structure of the bamboo but not its taper. The full potentials associated with the biomimicry of bamboo are hence not yet uncovered. Additionally, most of the previously reported bamboo-inspired lattice structures are highly directional and anisotropic. Therefore, in this study, inspired by all of the biological features of bamboo, the bamboo-inspired BCC (B-BCC) lattice structure with hollow and tapered struts was proposed. The strut geometry of the B-BCC lattice structure was determined by the degree of hollow and taper, and further influenced the mechanical properties of the B-BCC lattice structure. Using the homogenization method, the mechanical properties of B-BCC lattice structures with different geometric parameters and volume fractions were obtained. The effects of geometry on the elastic modulus, shear modulus, anisotropy, and deformation behavior of B-BCC lattice structures with different volume fractions were systematically investigated. Finally, a combination of artificial neural networks and elastic isotropy optimization was developed to obtain the isotropic B-BCC lattice structure with superior elastic modulus. The mechanical properties and failure behavior of the isotropic B-BCC lattice structure were investigated by compression experiments and the finite element method.

2. Material and methods

2.1 Lattice structures generation

The structure of bamboo is a typical lightweight structure that has a low density and excellent mechanical properties. The geometric structure of the bamboo pole is a hollow and tapered pillar,

as demonstrated in Fig. 1. Inspired by the geometry of the bamboo, the solid struts of BCC lattice structures were replaced by the hollow and tapered struts to improve the mechanical properties. Fig.1 illustrates the geometry of the novel bamboo-inspired BCC (B-BCC) lattice structure with hollow and tapered beams. A critical physical property of lattice structures is their volume fraction. We then proceed to derive the mathematical expression of the volume fraction of the B-BCC lattice structures. First, it is to note that the BCC lattice structure is obtained by the inner lattice structure subtracted from the outer one, as shown in Fig. 2(a). In this case, the volume fraction of the B-BCC lattice structure is simplified as:

$$\rho^* = \rho^*_{outer} - \rho^*_{inner} \tag{1}$$

Then, the ρ^*_{inner} was defined as a hollow parameter (α) to control the size of inner struts. For example, $\alpha = 0$ represent the B-BCC lattice structure with solid struts. Fig. 2(a) shows detail of the actual geometry of the outer structure. This structure composes of sixteen 1/8 nodes and eight struts, and the geometry of the 1/8 node is composed of one hexagonal pyramid and three trigonal pyramids. Therefore, the volume of the outer structure can be given:

$$V_{outer} = 16\sqrt{2}a^3 + 4\sqrt{3}(1+\beta+\beta^2)a^2 l \tag{2}$$

with $l = \frac{\sqrt{3}}{2}L - \sqrt{6}a$

where a is the side length of the equilateral hexagon base of the strut. β is the taper parameter that controls the side length of the equilateral hexagonal cross-section at the center of the strut, as shown in Fig. 2(a). l and L is the length of the strut and unit cell, respectively. The side length of the equilateral hexagonal cross-section at the center of the strut is $a\beta$. When $\beta = 1$, the taper strut would degrade into the uniform strut. Then the volume fraction of the B-BCC lattice structure can be modified as:

$$\rho^* = \frac{V_{outer}}{L^3} - \alpha = 6(1+\beta+\beta^2)\left(\frac{a}{L}\right)^2 - 12\sqrt{2}\left(\beta+\beta^2-\frac{1}{3}\right)\left(\frac{a}{L}\right)^3 - \alpha \tag{3}$$

In this study, α is explored within the range $[0, 0.95-\rho^*]$ with a step of 0.1, β is explored within the range $[0, 1]$ with a step of 0.1, and the ρ^* is set within the range $[0.05, 0.95]$ with a step of 0.05. The ρ^* and L were kept as constants, and different B-BCC lattice structures were generated by selecting different combinations of a, α, and β. 800 combinations were automatically generated and meshed using a Matlab code [50]. The models of B-BCC lattice structures with different geometric parameters (α and β) at $\rho^* = 0.15$ are demonstrated in Fig. 2(b).

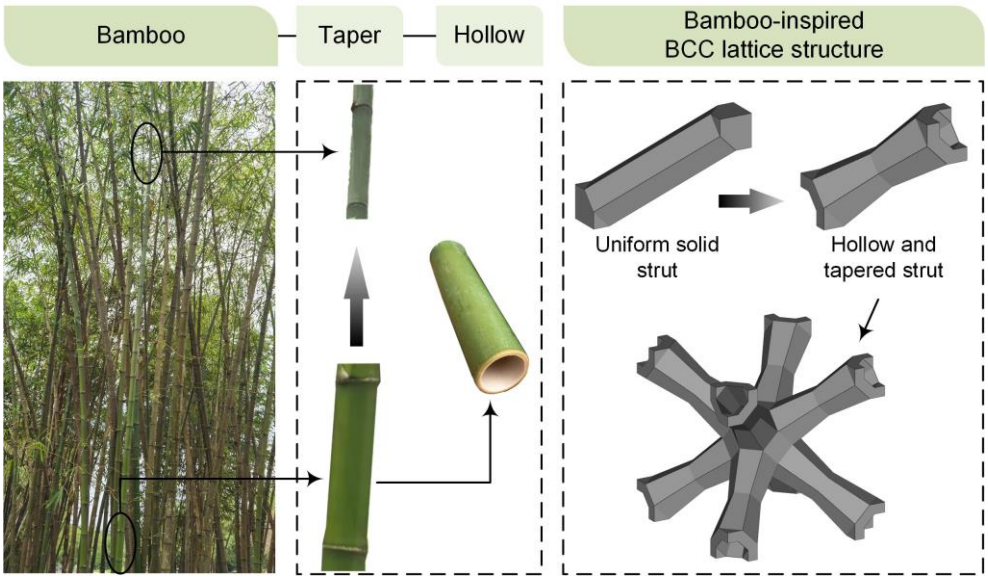

Fig. 1 Design evolution from bamboo to the bamboo-inspired BCC lattice structure.

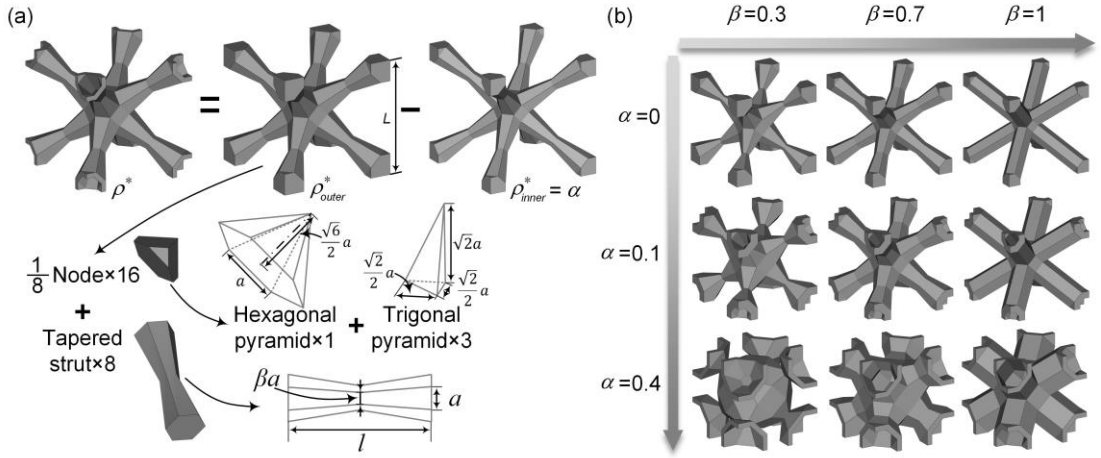

Fig. 2 (a) The geometry definition for the B-BCC lattice structure. (b) 3D models of the B-BCC unit cells with different geometric parameters at 0.15 volume fraction.

2.2 Homogenization procedure

To evaluate the elastic properties of the B-BCC lattice structure, a unit cell of the lattice structure was selected as the representative volume element (RVE). Periodic boundary conditions (PBCs) were applied to consider the effect of the adjacent unit cells. According to the PBCs, the displacement of the two opposite parallel RVE boundary surfaces can be expressed as [21]:

$$u_i(L_j) = u_i(0) + H_{ij}L_j \tag{4}$$

$$F_i(L_j) = -F_i(0) \tag{5}$$

where, u_i is the displacement, F_i is the force, H_{ij} is the displacement gradient, and L_j is the periodic length. The PBCs were then realized by applying multi-point constraints between the corresponding node pairs in Abaqus. The finite element models of the RVE were meshed with ten-node tetrahedral (C3D10) elements. Next, the homogenization method was used to calculate the equivalent elastic properties of lattice structures. The constitutive strain-stress relationship of lattice structures is denoted as $\boldsymbol{\sigma} = \boldsymbol{D\varepsilon}$, where $\boldsymbol{\sigma}$, $\boldsymbol{\varepsilon}$, and, $\boldsymbol{D}$ are macroscopic stress, strain, and equivalent elastic tensor, respectively. Because of the symmetry of the lattice unit cell, the constitutive relationship can be expressed as:

$$\begin{bmatrix}\sigma_{11}\\ \sigma_{22}\\ \sigma_{33}\\ \sigma_{23}\\ \sigma_{12}\\ \sigma_{13}\end{bmatrix}=\begin{bmatrix}D_{1111} & D_{1122} & D_{1122} & 0 & 0 & 0\\ D_{1122} & D_{1111} & D_{1122} & 0 & 0 & 0\\ D_{1122} & D_{1122} & D_{1111} & 0 & 0 & 0\\ 0 & 0 & 0 & D_{1212} & 0 & 0\\ 0 & 0 & 0 & 0 & D_{1212} & 0\\ 0 & 0 & 0 & 0 & 0 & D_{1212}\end{bmatrix}\begin{bmatrix}\varepsilon_{11}\\ \varepsilon_{22}\\ \varepsilon_{33}\\ \varepsilon_{23}\\ \varepsilon_{12}\\ \varepsilon_{13}\end{bmatrix} \tag{6}$$

The independent elasticity constants of the effective elastic matrix can be obtained by two loading cases, including a uniaxial strain loading and a shear strain loading.

Then, the elastic modulus (E), shear modulus (G), and Zener anisotropy index (A) are given:

$$E=\frac{D_{1111}^2+D_{1111}D_{1122}-2D_{1122}^2}{D_{1111}+D_{1122}} \tag{7}$$

$$G=D_{1212} \tag{8}$$

$$A=\frac{2D_{1212}}{D_{1111}-D_{1122}} \tag{9}$$

The Zener anisotropy index is used to evaluate the elastic anisotropy, and $A=1$ represents the elastic isotropy.

2.3 Isotropy optimization

To obtain the elastically isotropic lattice structures with high elastic modulus, the optimization problem is defined by minimizing the negative value of elastic modulus under the constraints of Zener anisotropy index and volume fraction. The design parameters α and β are the variables. The isotropy optimization problem is defined as:

$$\begin{cases} find\ \alpha,\beta \\ min\ -E=-\dfrac{D_{1111}^2+D_{1111}D_{1122}-2D_{1122}^2}{D_{1111}+D_{1122}} \\ s.t.\begin{cases} |A-1|=\left|\dfrac{2D_{1212}}{D_{1111}-D_{1122}}-1\right|\le 10^{-3} \\ \rho^*\le\rho_{cons} \\ \alpha_{min}\le\alpha\le\alpha_{max} \\ \beta_{min}\le\beta\le\beta_{max} \end{cases} \end{cases} \tag{10}$$

where, ρ_{cons} is the constraint of volume fraction, α_{min} and α_{max} is the lower and upper boundary of variable α, respectively. Similarly, β_{min} and β_{max} is the lower and upper value for β. Because the optimization problem is a constrained nonlinear optimization problem with two variables, the sequence quadratic programing (SQP) algorithm is used to solve the problem [51]. The termination criterion is defined as the relative objective function change in consecutive iterations less than 10^{-5}.

2.4 Isotropic performance validation

2.4.1 Multi-layer simulation

To verify the isotropy of the B-BCC lattice structures, the elastic modulus in the [001] and [011] directions were compared using Abaqus. The [001] and [011] samples were composed of $5\times5\times5$ and $5\times5\sqrt{2}\times5\sqrt{2}$ unit cells, respectively. The size of the unit cell is $5mm$. The [011] samples can be obtained by rotating the [001] samples 45 degrees around the *x*-axis, as demonstrated in Fig. 3(a). The lattice samples were meshed with C3D10 elements. The samples were subjected to a displacement at the top surface equivalent to 0.01 of the height of the sample, and the bottom surface was fixed in z-direction using the ZSYMM boundary condition [52], as shown in Fig. 3(b). The constituent material was assumed to be a linear isotropic elastic model with an elastic modulus of $1993.4MPa$ and Poisson's ratio of 0.3.

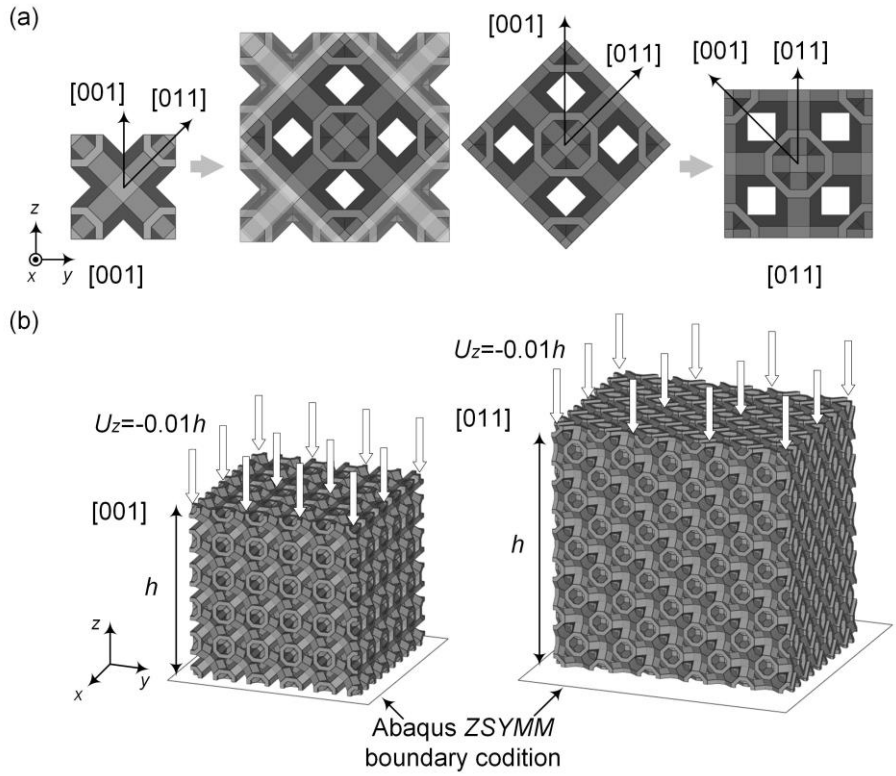

Fig. 3 (a) Schematic of the unit cell for [001] and [011] orientations. (b) The boundary conditions for the multi-layer simulation.

2.4.2 Sample fabrication

The optimized B-BCC lattice structures with 0.2 volume fractions were selected to be fabricated by digital light processing (DLP). The size of the samples was the same as that of the simulation models. Correspondingly, the isotropic BCC lattice structures with hollow struts ($\beta = 1$) and original BCC lattice structures ($\alpha = 0$ and $\beta = 1$) were also considered. A commercial DLP 3D printer, Asiga Max X27, using the Nova3D photosensitive resin, was used to manufacture the samples. The key processing parameters include a layer thickness of $50\mu m$, exposure time of $1.1s$, and light intensity of $5mWcm^{-2}$. Subsequently, the as-printed samples were then cured for $1h$ in the Asiga Flash curing chamber. The fabricated samples are illustrated in Fig. 4.

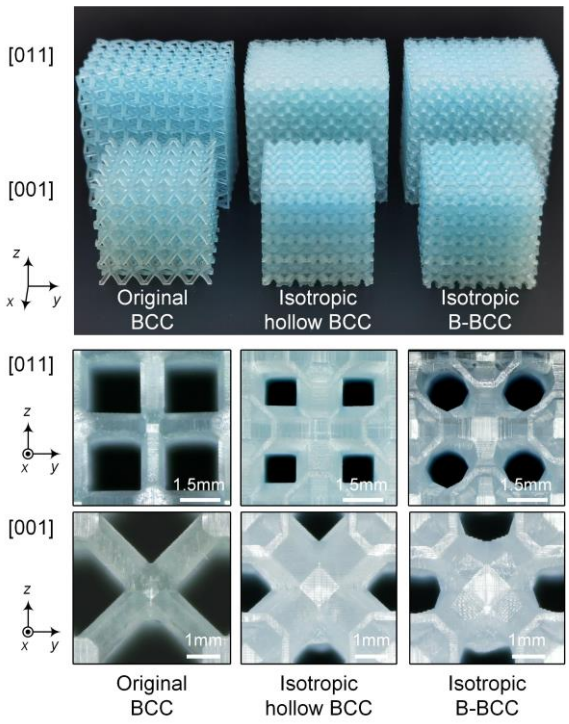

Fig. 4 The lattice samples fabricated by DLP.

2.4.3 Compression test

A commercial universal mechanical testing machine (Shimadzu AG25-TB) was used for compression tests. Two duplications of each sample were tested. The upper load cell moved downwards at a speed of $2mm/min$. The load and displacement data were recorded and used to calculate the strain-stress curves. The stress (σ) was obtained by dividing the compressive force into the apparent cross-sectional area (length×width) of the samples, and the strain (ε) was defined as the ratio of displacement and initial height of the samples.

3. Results and discussion

3.1 Elastic properties

The mechanical properties of B-BCC lattice structures obtained by the homogenization method are shown in Fig. 5. These values are also compared with the Hashin-Shtrikman (HS) upper bounds, which are the highest theoretically achievable mechanical properties for a porous structure [53]. It can be seen from Figs. 5(a) and (b) that the elastic modulus and shear modulus of B-BCC lattice structures gradually improved with the increase of the volume fraction. Although the values of all designs fall below the HS upper bound, designs that are very close to the HS upper bound can be found for all volume fractions. Therefore, the mechanical properties of B-BCC lattice structures can be optimized by adjusting the geometry parameters (α and β). The unit cells with the highest elastic modulus and shear modulus at different volume fractions in homogenization results are shown in Figs. 5(a) and (b), respectively. The results show that the design of hollow struts is beneficial to the improvement of elastic modulus, while the design of solid struts is beneficial to the shear modulus. In addition, the appropriate taper design can improve both the elastic modulus and the shear modulus.

Fig. 5(c) shows the Zener anisotropy index (A) of B-BCC lattice structures. $A = 1$ represents an elastically isotropic structure. It can be found that the values of A are close to 1 for B-BCC

lattice structures with high volume fractions. This is because the structures with high volume fractions were like solid material with holes in them, and the topology configuration of lattice structures less influenced their anisotropy characteristic. A similar phenomenon was also observed in other lattice structures, such as octet and plate cubic [54]. As shown in Fig. 4(c), the $A = 1$ is in the range of A values of the samples for all volume fractions, which means that the elastically isotropic B-BCC lattice structures can be obtained by controlling the geometric parameters. Further analysis of the samples with a 0.2 volume fraction shows that the strongest direction of the original BCC lattice structure ($\alpha = 0,\ \beta = 1$) was the diagonal direction, and the uniaxial direction was the weakest. This is due to the arrangement of the struts that all struts are oriented in diagonal directions. Although the design of tapered struts can weaken the diagonal performance and improve the axial performance to reduce the anisotropy, it is still difficult to obtain elastic isotropy. However, the α effectively influenced the anisotropy property, and the strongest and weakest directions were reversed by increasing the α, leading to a relatively balanced stiffness at $\alpha = 0.3$.

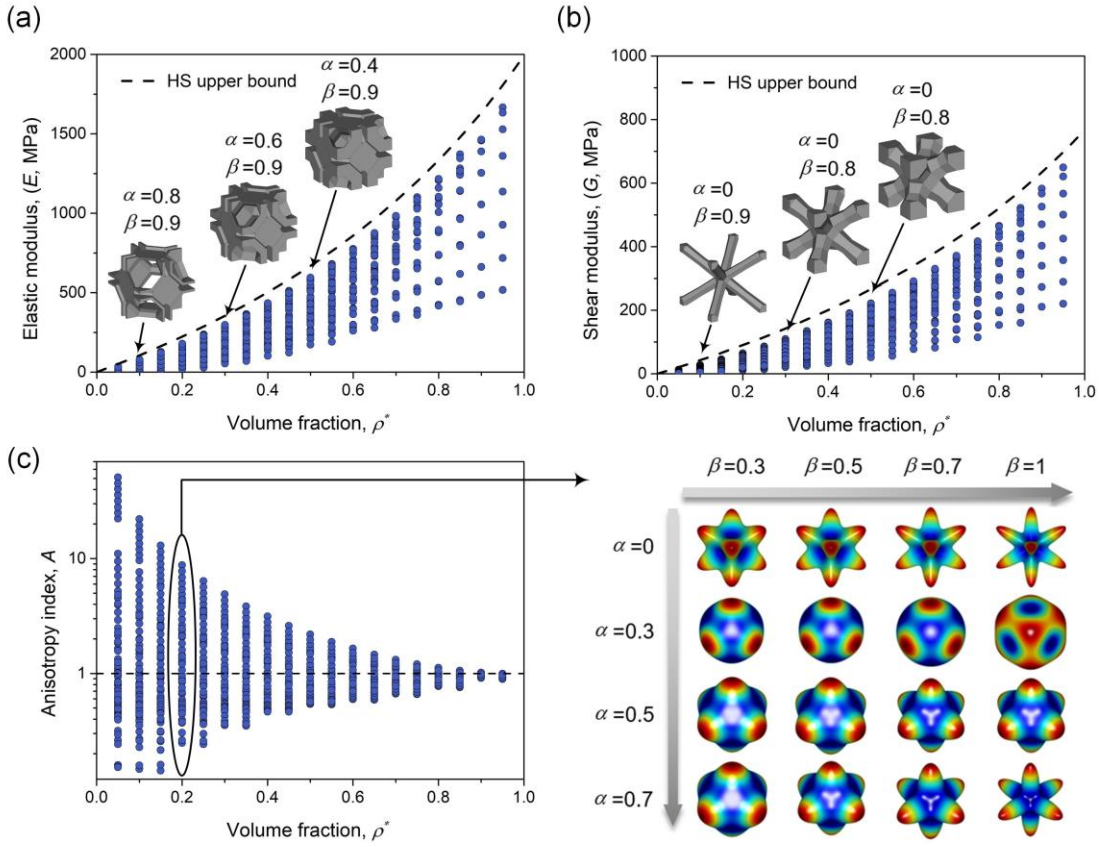

Fig. 5 The (a) elastic modulus, (b) shear modulus, and (c) anisotropy index for all B-BCC lattice structures obtained from numerical homogenization.

To illustrate the influence of geometric parameters (α and β) on mechanical properties, the smoothened figures of the B-BCC at 0.1, 0.2, and 0.5 volume fractions are shown in Fig. 6. For the elastic modulus, the large α significantly improved the elastic modulus of B-BCC lattice structures. Especially at the 0.1 volume fraction, the hollow design ($\alpha = 0.8,\ \beta = 1$) increases the elastic modulus by more than 1900% when compared to the original one ($\alpha = 0,\ \beta = 1$). With regards to β, the elastic modulus of the B-BCC lattice structures with small taper slightly increased with the decrease of β. Although these two geometric parameters can improve the elastic modulus, the reasons are different. Principally, the α changed the deformation behavior and the moment of

inertia, while the β only improved the stress distribution, which will be further discussed in Section 3.2. In addition, as the volume fraction increased, the α and β showed less effects on the elastic modulus. For example, the ratio between the maximum and minimum elastic modulus (E_{max}/E_{min}) of B-BBC lattice structures with 0.1 and 0.5 volume fractions was 21.16 and 3.43, respectively. One may assign it to the fact that with the increase of the volume fraction, the structure more presents the properties of solid materials with holes, and thus the geometry exhibited little influence on the uniaxial response.

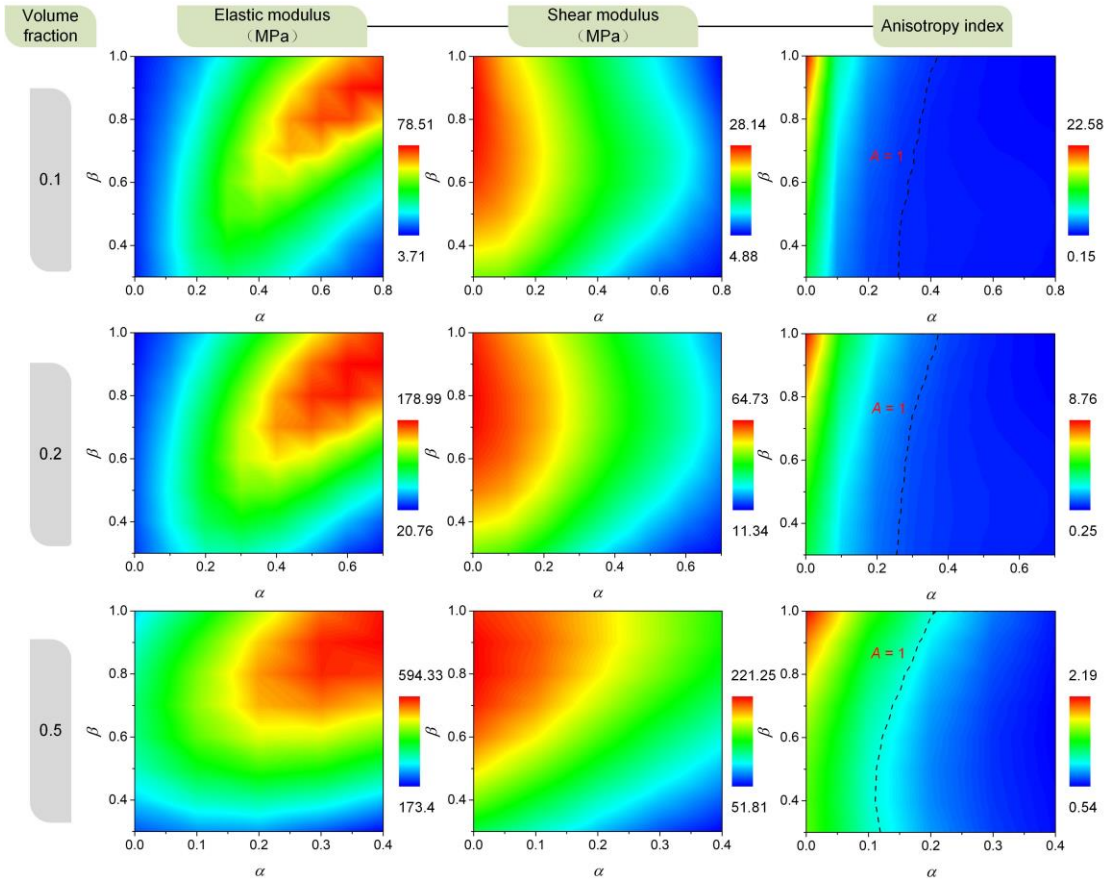

Fig. 6 Contour plots of the elastic modulus, shear modulus, and anisotropy index of the B-BCC lattice structures with relative volume 0.1, 0.2, and 0.5, for varying geometric parameters.

Under the shear load, the slight taper was beneficial, but the hollow design ($\alpha > 0$) weakened the shear modulus, as shown in Fig. 6. Similarly, the ratio of the maximum to minimum shear modulus (G_{max}/G_{min}) gradually decreased with the increase of the volume fraction, but the values of the ratio for shear modulus were lower than that for elastic modulus at low volume fractions. For example, at 0.1 volume fraction, the G_{max}/G_{min} was only 5.77, while E_{max}/E_{min} was 21.16. This is because the geometric parameters changed the deformation behavior of B-BCC lattice structures under the uniaxial load but rarely influenced the deformation behavior under the shear load. The influence of the geometric parameters on shear modulus and deformation behaviors will be discussed in Section 3.2.

The effect of the geometric parameters on anisotropy is shown in Fig. 6. It can be observed that the elastically isotropic B-BCC lattice structure ($A = 1$) can be obtained for all β values, which means that the anisotropic property was mainly determined by changes of α. It is basically attributed to the fact that α reversed the strongest and weakest directions, while β only slightly

strengthened the weakest directions and weakened the strongest directions, as shown in Fig. 5 (c).

3.2 Deformation behavior

Due to the complex internal configuration of the B-BCC unit cell, the deformation behavior (bending or stretching) was difficult to be characterized by the Maxwell stability criterion [11]. Therefore, the Gibson-Ashby model was introduced to evaluate the deformation behavior [10]. According to the Gibson-Ashby model, the relationship between relative mechanical properties and volume fractions can be expressed as:

$$\frac{E}{E_S} = C_1(\rho^*)^{n_1} \tag{11}$$

$$\frac{G}{E_S} = C_2(\rho^*)^{n_2} \tag{12}$$

where, E_S is the elastic modulus of the bulk material. The C_1, C_2, n_1, and n_2 are fitted proportionality constants and exponents. The predicted exponent depends on whether the structure is bending- or stretch-dominated, i.e., the exponent value of ~2 for bending-dominated and ~1 for stretch-dominated. In this work, only the designs covered 0.05 – 0.3 volume fractions were considered for investigation. The fitted values of the exponents are shown in Fig. 7, and the coefficients of determination (R^2) of the fitted results are higher than 0.999.

It can be observed that increasing α and decreasing the β can gradually change the deformation behavior of B-BCC lattice structures from bending-dominated ($n_1 = 2.64$) to stretching-dominated ($n_1 = \sim 1$) under the uniaxial load. However, the change in geometric parameters had little effect on the values of n_2. The n_2 varied in a small range of 0.91–1.34, indicating the deformation behavior of the B-BCC lattice structures mainly was stretching-dominated under the shear load. This difference is attributed to the topology configuration of BCC, in that the struts were aligned in the diagonal directions. To further analyze the deformation behavior, the Mises stress distributions of the B-BCC unit cell with different geometric parameters under different loading conditions are demonstrated in Figs. 8(a) and (b).

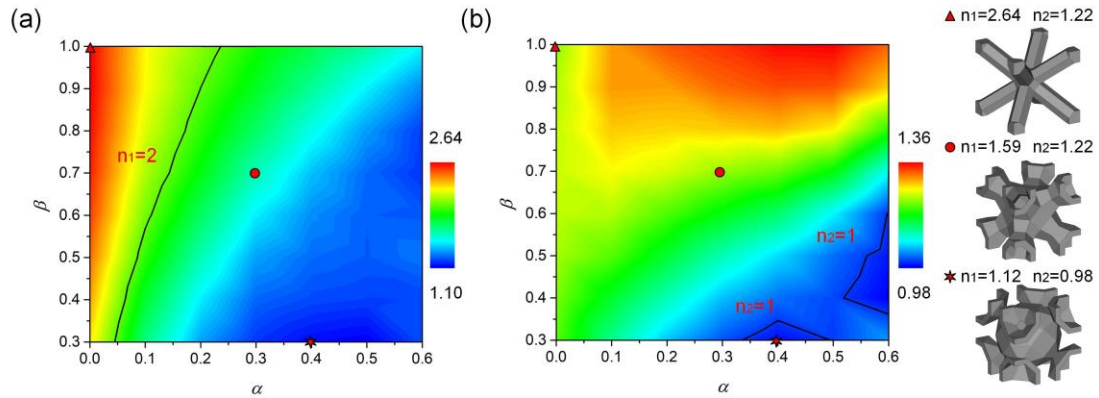

Fig. 7 Contour plots of the fitted exponents (a) n_1 and (c) n_2 of the B-BCC lattice structures with variation of geometric parameters.

Under the uniaxial compression load, the original BCC lattice structure ($\alpha = 0$, $\beta = 1$) belongs to bending-dominated ($n_1 = 2.64$), and the Misses stress mainly concentrated at the node region due to the bending of the struts, as shown in Fig. 8 (a). Then, the stress was gradually changed from the node region to the center of the struts by decreasing the β. Therefore, a slight taper is beneficial for elastic modulus, but a large taper will induce stress concentrations on the node and decrease the elastic modulus. To clearly demonstrate the geometric effects on deformation behavior,

the principal stress distributions of RVE are demonstrated in Fig. 9(a). The red arrows represent the tensile stress and the blue ones represent the compressive stress. In general, the principle stress distribution in uniform and tapered struts was similar. The compressive and tensile stress was mainly displayed at the concave and convex of the struts, respectively, which is a typical deformation behavior of bending of the struts. However, when α was increased, more stress at the node region was distributed in the presence of vertical plates (e.g. at $\alpha = 0.4,\ \beta = 1$), and more compressive stresses were parallel to the load direction. For this reason, the deformation behavior gradually changed from bending-dominated to stretching-dominated, which is consistent with the fitting results in Fig. 7(a). Moreover, because the moment of inertia of the hollow struts ($\alpha > 0$) is higher than that of solid struts ($\alpha = 0$), the elastic modulus was significantly improved simultaneously. Compared to the methods that control deformation behaviors and improve stiffness under uniaxial compression load by changing the lattice topology [55, 56], adding additional struts [30], or combing different lattice structures [57], the B-BCC design provides a novel way to control the deformation behavior and stiffness without changing the topology configuration.

Under the shear load, the original BCC lattice structure ($\alpha = 0,\ \beta = 1$) belongs to stretching-dominated ($n_2 = 1.22$), and the Misses stress uniformly distributed on struts due to the tension or compression of the struts, as shown in Fig. 8(b) and Fig. 9(b). It is noteworthy that the Misses stress distribution of RVE changed little with the increase of α, and the maximum stress gradually transferred from the node region to the center of the strut with the decrease of β. Meanwhile, the compressive and tensile stress was mainly parallel to the struts when α and β changed, as shown in Fig. 9(b). Thus, the deformation behavior of the B-BCC lattice structures was little influenced by α and β. However, as aforementioned, the shear modulus was more sensitive to the change of α than β. It can be observed that the tensile and compressive stresses were uniformly along the struts for the original BCC lattice structure. For this reason, the original BCC lattice structure has a superior shear modulus. It is clear from Fig. 9(c) that the principal stress distributions were less sensitive to the change of β than α. When the α increased, the principal stress distributions became more complex, and each strut displayed a combination of tensile and compressive stresses. These findings explain the observation in Fig.6 that the shear modulus was largely reduced by increasing α but less influenced by changing β.

Interestingly, when $\alpha = 0.4$ and $\beta = 0.3$, the n_1 and n_2 values were both ~1, which means that the deformation behavior of this structure was stretching-dominated under the uniaxial compression load and shear load. However, the stretching-dominated deformation behavior might not be governed by the material's alignment in the loading direction but due to the geometry of the center of the struts. As shown in Fig. 8, the stress was more concentrated at the center of the struts, and the lattice structure might resist the uniaxial compression and shear load through the local tension and compression deformation at the center of the struts. Therefore, although this structure belongs to a stretching-dominated structure, its elastic modulus and shear modulus were relatively lower than many more bending-dominated B-BCC lattice structures, as shown in Fig. 6.

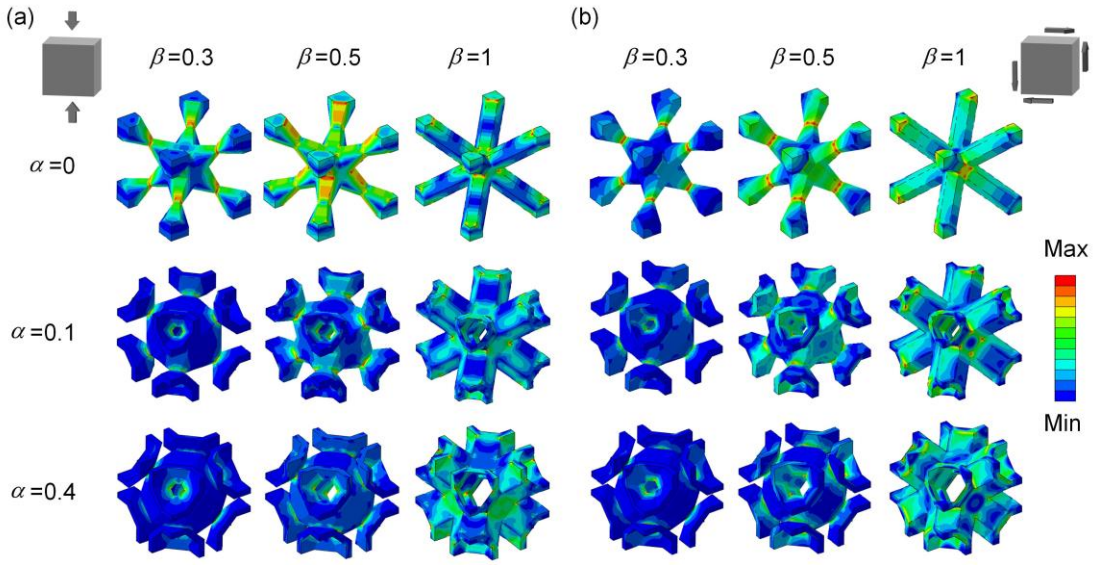

Fig. 8 The geometric effects on Misses stress distribution of RVE with 0.2 volume fraction at (a) $\varepsilon_{33} = 0.01$ and (b) $\varepsilon_{23} = 0.01$.

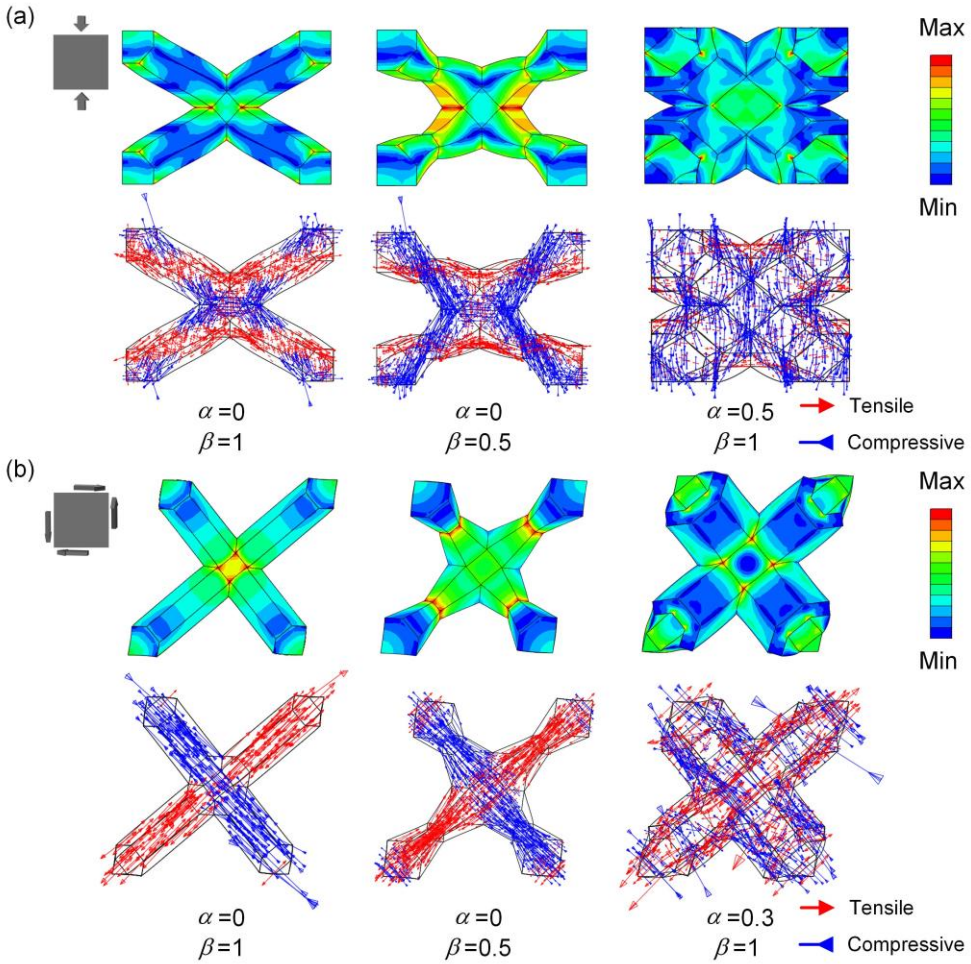

Fig. 9 The Misses stress and principal stress distribution of RVE at (a) $\varepsilon_{33} = 0.01$ and (b) $\varepsilon_{23} = 0.01$ with a deformation scale factor ×20.

3.3 Isotropy optimization

As noticed, the elastic modulus of the B-BCC lattice structure can be adjusted by α and β, and the elastic anisotropy was dependent on the combination of α and β. In structural components, the elastically isotropic ensures the lattice structures effectively resist the complex load conditions. Therefore, an isotropy optimization approach was proposed to design the B-BCC lattice structures with elastic isotropy and high elastic modulus simultaneously. The flowchart of the optimization process is summarized in Fig. 10.

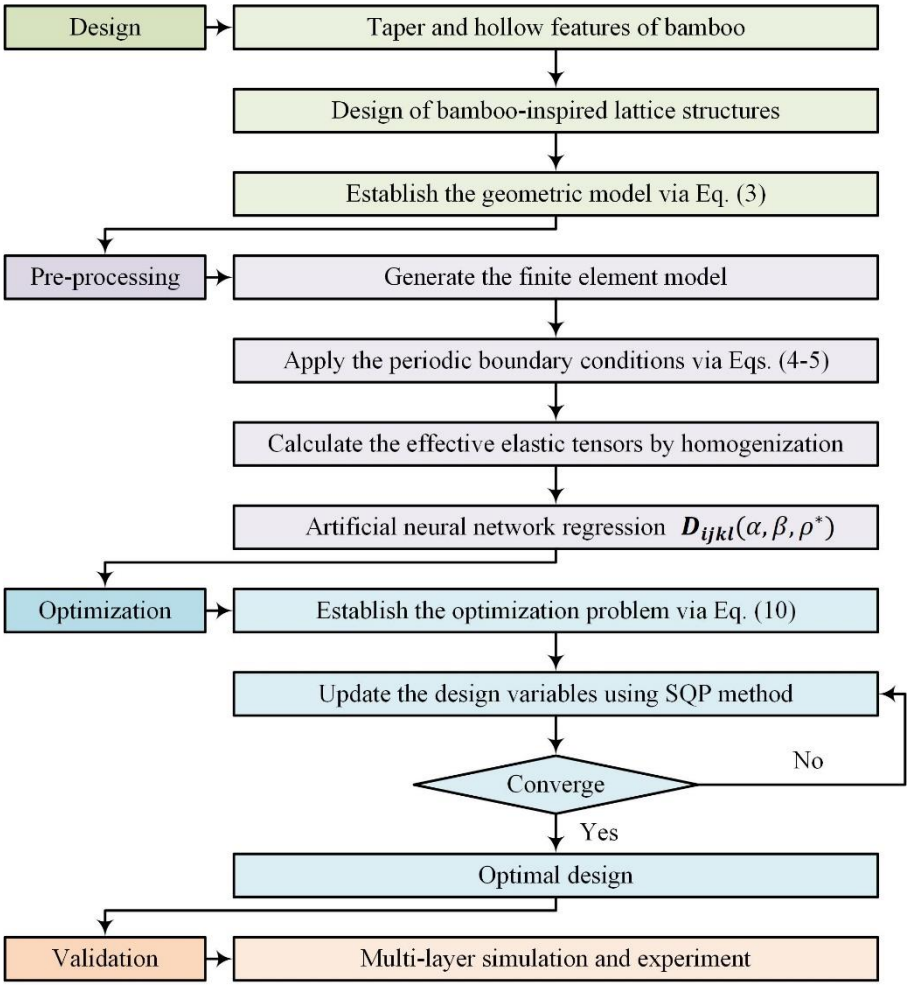

Fig. 10 The flowchart of the elastic isotropy optimization process of B-BCC lattice structures.

Firstly, the bamboo-inspired lattice structures with different geometric parameters and volume fractions were generated by Eq. (3). Secondly, to avoid the tedious homogenization calculation during the iterative process for optimization, the relationships between the geometric parameters (α and β), volume fraction (ρ^*), and the elasticity constants (D_{ijkl}) should be developed. Considering the complexity of the nonlinear relationships, a two-layer (1 hidden layer and 1 output layer) artificial neural network (ANN) was applied to establish the relationships, as illustrated in Fig. 11(a). The number of hidden neurons was 20 to ensure the R^2 of the predicted results were higher than 0.999. The data were randomly divided into training set (70%), validation set (15%), and testing set (15%). The Levenberg-Marquardt (LM) algorithm was adapted to train the ANN [58]. The predicted and simulated values of elasticity constants at 0.2 volume fraction are illustrated in Fig. 11(b). It can be observed that the predicted curved surfaces successfully went across the simulated data, indicating high accuracy of the predicted results. Thirdly, the optimization problem was established and solved by the SQP algorithm using Matlab code. Finally, the optimization results were validated

by the multi-layer simulation and experiment.

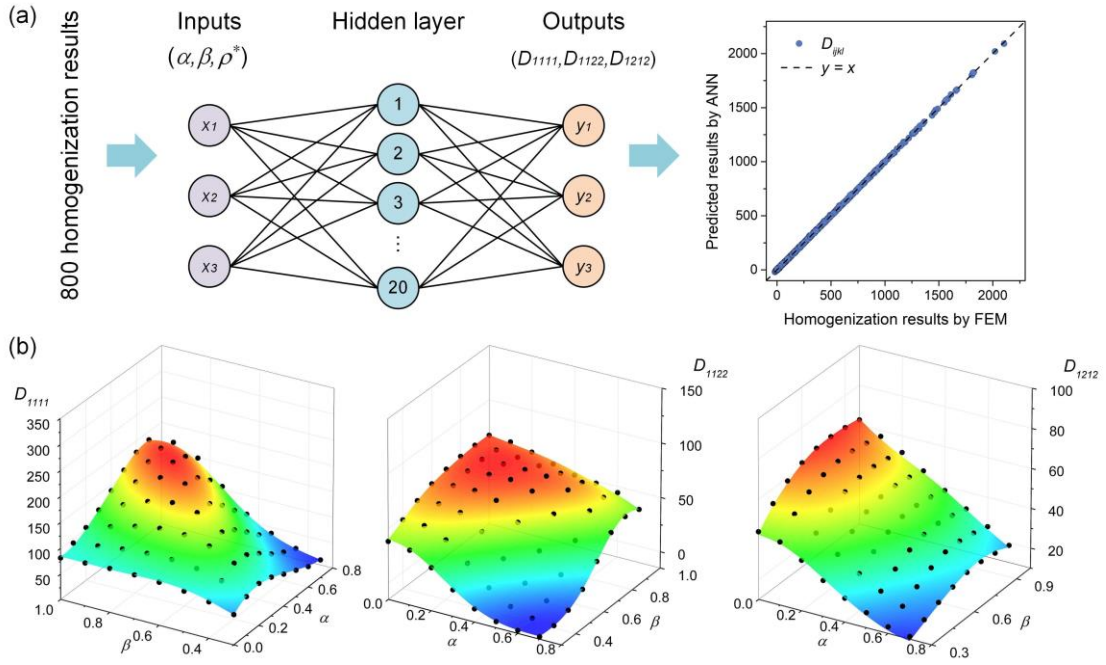

Fig. 11 (a) Diagram of ANN architecture and the high accuracy achievable from the trained network. (b) Predicted surfaces of the effective elastic constants for B-BCC lattice structures with 0.2 volume fraction.

Using the isotropy optimization approach, the elastically isotropic B-BCC lattice structures with 0.1, 0.2, and 0.3 volume fractions were obtained. The optimization iteration process is shown in Figs. 12(a-c), and the final results are listed in Table 1. Then, the results were compared with the elastic modulus of isotropic hollow BCC and the original BCC lattice structures under the uniaxial compression load ([001] direction), as demonstrated in Fig. 12(d). It is apparent that the elastic modulus of the optimized isotropic B-BCC lattice structure is the highest and closest to the HS upper bound. The elastic modulus increased by 271.24%-1335% compared with the original BCC lattice structures. It was of interest to compare the bamboo-inspired strategy in this study with other optimized designs of BCC lattice structures. For example, Chen et al. [29] used rotation and mirror operations to create a modified BCC lattice structure, and the elastic modulus of lattice structures was improved by 552%. Bai et al. [28] proposed a type of BCC lattice structure with curved struts and increased the elastic modulus by 213.7%. Maskery et al. [59] added a vertical strut to the BCC lattice unit cell and generate the BCC-Z lattice structures. The elastic modulus of BCC-Z lattice structures was 218% higher than that of original BCC lattice structures. Tancogne-Dejean et al. [25] designed the BCC lattice structures with taper struts, and the uniaxial compression tests demonstrated that the use of tapered struts increased the elastic modulus up to 70%.

It should be noted that the optimized B-BCC lattice structure had high elastic modulus and elastic isotropy, which means this structure had high stiffness in all directions. Moreover, compared to the isotropic hollow BCC which mimics the hollow structure of bamboo, the optimized B-BCC which considers the hollow and taper structure of bamboo further improved the elastic modulus increased by 17.72%-43.63%.

Table 1 The isotropy optimization results of B-BCC lattice structures.

ρ^*	α	β	**Elastic modulus (MPa)**	**Anisotropy index**
0.1	0.364	0.699	53.21	~1
0.2	0.308	0.730	129.84	~1
0.3	0.254	0.758	224.72	~1

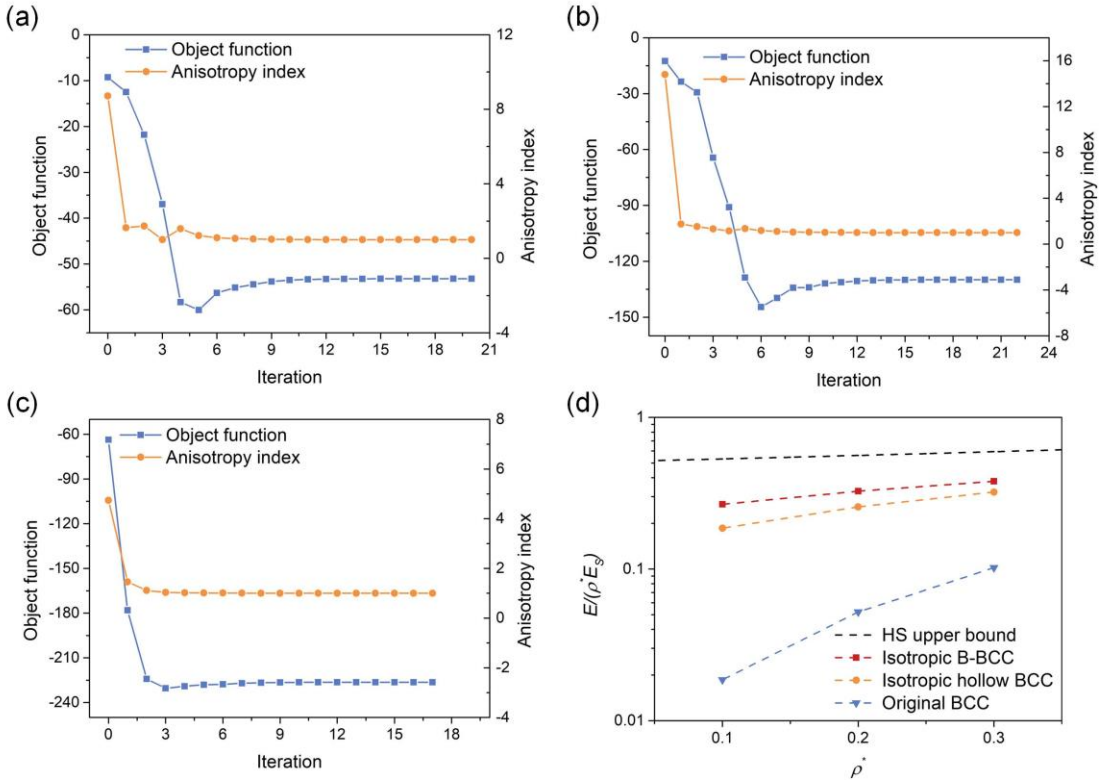

Fig. 12 Iteration histories of optimization process at (a) $\rho_{cons} = 0.1$, (b) $\rho_{cons} = 0.2$, and (c) $\rho_{cons} = 0.3$. (d) Normalized elastic modulus as a function of the relative density of different lattice structures.

3.4 Isotropic performance validation

The experimental strain-stress curves of the lattice samples are demonstrated in Fig. 13. Three distinct regions are observed in strain-stress curves, including the elastic-plastic stage, plateau stage, and densification stage. For original BCC samples, the difference between strain-stress curves at the elastic-plastic stage was large in the [100] and [110] directions. This was mainly caused by the elastic anisotropy of original BCC lattice structures. After the stress reached the initial stress peak, the load-bearing capability of the original BCC samples rapidly decreased. This is due to the shear failure observed in the inset images in Fig. 13(a), and the samples subsequently separated and slid with low load-bearing capability. The diagonal or V-shaped shear bands were also found in other types of strut-based lattice structures, such as FCC [28], F2BCC [60], and gyroid [61]. In addition, a similar phenomenon was also observed in BCC lattice structures made of different brittle materials, such as Ti-6Al-4V [20, 27, 28]. It should be noted that shear band failure is a common failure mechanism for bending-dominated lattice structures [62]. In contrast, a totally different failure behavior was observed for isotropic hollow BCC and isotropic B-BCC samples in Fig. 13(b) and (c). The samples exhibited an initial top layer collapse followed by a layer-by-layer failure. This distinct failure mechanism enables the samples to maintain relatively high load-bearing capacity after failure, which is beneficial for energy-absorbing applications. There are two likely causes for

the distinct failure mechanism. Firstly, the hollow design increased the moment of inertia of struts, making a more stretching-dominated deformation behavior for isotropic hollow BCC and isotropic B-BCC samples. The layer-by-layer failure is a common failure mechanism for stretching-dominated lattice structures [62]. Secondly, the tapered design improved the node region and weaken the region of the center of the strut. The tapered geometry of the strut changed the stress distribution, leading to a local collapse in the strut [21, 25, 26]. Interestingly, although the isotropic B-BCC lattice structure is elastically isotropic, the stress values of stress-strain curves at the plastic stage were almost the same in the [001] and [011] directions. Because the B-BCC lattice structures provide a variety of geometric parameters for elastically isotropic designs without changing the volume fraction, the lattice structures with elastic-plastic isotropy or even isotropic energy absorption capacity might be realized by adjusting the geometric parameters.

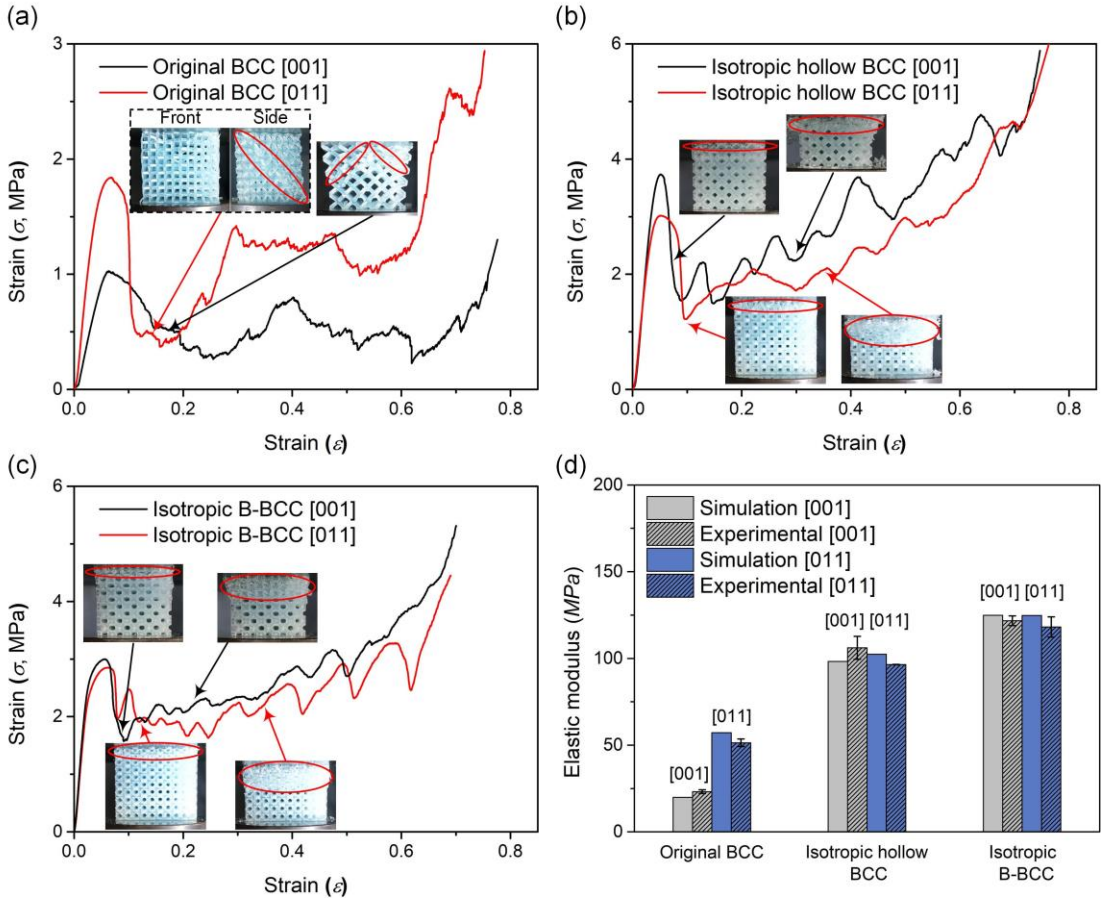

Fig. 13 The strain-stress curves of the (a) original BCC, (b) isptropic hollow BCC, (c) isotropicB-BCC lattice samples with 0.2 volume fraction in [001] and [011] directions. (c) The multi-layer simulation and experimental results.

The elastic modulus of the lattice samples obtained from multi-layer simulation and experiment are summarized in Fig. 13(d). It can be found that the elastic modulus of original BCC samples greatly differed in the [001] and [011] directions, while the elastic modulus of isotropic hollow BCC and isotropic B-BCC samples was close in the [001] and [011] directions. Moreover, the isotropic B-BCC samples showed the highest elastic modulus, which is consistent with the optimization results. The predicted elastic modulus was in good agreement with the experiment results, with relative errors of 2.51%-16.67%. It is worth noting that for isotropic samples, the elastic modulus was slightly different in the [001] and [011] directions for both multi-layer simulation and

experiment results. This is reasonable because the homogenization method assumes that the macroscale structure is sufficiently larger than the size of the lattice unit cell [21, 22], while the lattice samples used in the multi-layer simulation and experiment contained $5 \times 5 \times 5$ and $5 \times 5\sqrt{2} \times 5\sqrt{2}$ unit cells. Therefore, the different number of unit cells might influence the elastic modulus of lattice structures [22]. A similar phenomenon was also found in other studies of isotropic lattice structures [48]. In general, the isotropic B-BCC lattice structure showed the highest elastic modulus, and the deviation in different directions is less than 0.06%, and 3.01% for multi-layer simulation and experiment, respectively, which validates the effectiveness of the proposed elastic isotropy optimization approach.

4. Conclusions

In this study, a novel class of bamboo-inspired BCC (B-BCC) lattice structures with tapered and hollow struts was proposed. The mechanical properties and deformation behavior of the B-BCC lattice structures with different geometry of hollow and tapered struts were investigated based on the representative volume element with periodic boundary conditions. Moreover, an artificial neural network was used to establish the relationship between geometric parameters (α and β), volume fraction (ρ^*), and the elasticity constants (D_{ijkl}), and an elastic isotropy optimization approach was proposed to obtain the isotropic B-BCC lattice structures with high elastic modulus. Finally, the optimized samples were compared to the original BCC and isotropic hollow BCC lattice structures by multi-layer simulation and compression tests. The main conclusions of this study can be summarized as follows:

(1) The elastic modulus and shear modulus of the B-BCC lattice structures can be widely controlled by geometric parameters (α and β), and the highest mechanical properties of B-BCC lattice structures were near the HS upper bounds.

(2) The elastically isotropic B-BCC lattice structure can be obtained for all volume fractions. The anisotropy characteristic was mainly determined by α, and the strongest and weakest directions were reversed when increasing α.

(3) The geometric parameters significantly influenced the deformation behavior of B-BCC lattice structures (from bending- to stretching-dominated) under uniaxial compression load but rarely influenced the deformation behavior under shear load.

(4) The isotropic B-BCC lattice structures with high elastic modulus were obtained through isotropy optimization. Compared with the original BCC and isotropic hollow BCC lattice structures with equal volume fractions, the elastic modulus increased by 271.24%-1335% and 17.72%-43.63%, respectively.

(5) The optimized results were confirmed through multi-layer simulation and compression experiments. The variations between the elastic modulus at the [100] and [110] directions were less than 3.01% for the isotropic B-BCC lattice structure.

The proposed B-BCC lattice structures enable tunable mechanical properties and deformation behaviors by adjusting geometric parameters, which provides a novel bio-inspired strategy to design lightweight architectures with desired properties for engineering applications. In future work, the plastic characteristics of the B-BCC lattice structures will be investigated, and the optimization approach will consider the plastic properties to reduce the plastic anisotropy of B-BCC lattice structures.

Acknowledgments

This work is supported by MOE AcRF Tier 1 FRC Research Grant (A-0009123-01-00) and China Scholarship Council (202006050088).

Declarations of interest

The authors declare that they have no known competing financial interests or personal relationships that could have appeared to influence the work reported in this paper.

Reference

[1] L.-Y. Chen, S.-X. Liang, Y. Liu, L.-C. Zhang, Additive manufacturing of metallic lattice structures: Unconstrained design, accurate fabrication, fascinated performances, and challenges, Materials Science and Engineering: R: Reports 146 (2021) 100648.
[2] T. Tancogne-Dejean, M. Diamantopoulou, M.B. Gorji, C. Bonatti, D. Mohr, 3D Plate-Lattices: An Emerging Class of Low-Density Metamaterial Exhibiting Optimal Isotropic Stiffness, Adv Mater 30(45) (2018) 1803334.
[3] M. Mahbod, M. Asgari, C. Mittelstedt, Architected functionally graded porous lattice structures for optimized elastic-plastic behavior, Proceedings of the Institution of Mechanical Engineers, Part L: Journal of Materials: Design and Applications 234(8) (2020) 1099-1116.
[4] N. Qiu, J. Zhang, F. Yuan, Z. Jin, Y. Zhang, J. Fang, Mechanical performance of triply periodic minimal surface structures with a novel hybrid gradient fabricated by selective laser melting, Engineering Structures 263 (2022) 114377.
[5] X. Li, X. Yu, J.W. Chua, H.P. Lee, J. Ding, W. Zhai, Microlattice Metamaterials with Simultaneous Superior Acoustic and Mechanical Energy Absorption, Small 17(24) (2021) 2100336.
[6] T. Dixit, P. Nithiarasu, S. Kumar, Numerical evaluation of additively manufactured lattice architectures for heat sink applications, International Journal of Thermal Sciences 159 (2021) 106607.
[7] X. Li, X. Yu, W. Zhai, Additively Manufactured Deformation-Recoverable and Broadband Sound-Absorbing Microlattice Inspired by the Concept of Traditional Perforated Panels, Adv Mater 33(44) (2021) 2104552.
[8] F. Liu, T. Zhou, T. Zhang, H. Xie, Y. Tang, P. Zhang, Shell offset enhances mechanical and energy absorption properties of SLM-made lattices with controllable separated voids, Materials & Design 217 (2022) 110630.
[9] M. Zhao, D.Z. Zhang, F. Liu, Z. Li, Z. Ma, Z. Ren, Mechanical and energy absorption characteristics of additively manufactured functionally graded sheet lattice structures with minimal surfaces, International Journal of Mechanical Sciences 167 (2020) 105262.
[10] L.J. Gibson, Ashby, M.F., Cellular Solids: Structure and Properties, Cambridge University Press, Cambridge (1997).
[11] J.C. Maxwell, L. On the calculation of the equilibrium and stiffness of frames, The London, Edinburgh, and Dublin Philosophical Magazine and Journal of Science 27(182) (1864) 294-299.
[12] F.N. Habib, P. Iovenitti, S.H. Masood, M. Nikzad, Fabrication of polymeric lattice structures

for optimum energy absorption using Multi Jet Fusion technology, Materials & Design 155 (2018) 86-98.
[13] R. Gümrük, R.A.W. Mines, Compressive behaviour of stainless steel micro-lattice structures, International Journal of Mechanical Sciences 68 (2013) 125-139.
[14] R. Gümrük, R.A.W. Mines, S. Karadeniz, Static mechanical behaviours of stainless steel micro-lattice structures under different loading conditions, Materials Science and Engineering: A 586 (2013) 392-406.
[15] L. Yang, Y. Li, Y. Chen, C. Yan, B. Liu, Y. Shi, Topologically optimized lattice structures with superior fatigue performance, International Journal of Fatigue 165 (2022) 107188.
[16] R.A.W. Mines, S. Tsopanos, Y. Shen, R. Hasan, S.T. McKown, Drop weight impact behaviour of sandwich panels with metallic micro lattice cores, International Journal of Impact Engineering 60 (2013) 120-132.
[17] M. Teimouri, M. Asgari, Mechanical performance of additively manufactured uniform and graded porous structures based on topology-optimized unit cells, Proceedings of the Institution of Mechanical Engineers, Part C: Journal of Mechanical Engineering Science 235(9) (2020) 1593-1618.
[18] V. Crupi, E. Kara, G. Epasto, E. Guglielmino, H. Aykul, Static behavior of lattice structures produced via direct metal laser sintering technology, Materials & Design 135 (2017) 246-256.
[19] U.A. Dar, H.H. Mian, M. Abid, A. Topa, M.Z. Sheikh, M. Bilal, Experimental and numerical investigation of compressive behavior of lattice structures manufactured through projection micro stereolithography, Materials Today Communications 25 (2020) 101563.
[20] L. Bai, J. Zhang, Y. Xiong, X. Chen, Y. Sun, C. Gong, H. Pu, X. Wu, J. Luo, Influence of unit cell pose on the mechanical properties of Ti6Al4V lattice structures manufactured by selective laser melting, Additive Manufacturing 34 (2020) 101222.
[21] M. Zhao, D.Z. Zhang, Z. Li, T. Zhang, H. Zhou, Z. Ren, Design, mechanical properties, and optimization of BCC lattice structures with taper struts, Composite Structures 295 (2022) 115830.
[22] X. Wang, L. Zhu, L. Sun, N. Li, Optimization of graded filleted lattice structures subject to yield and buckling constraints, Materials & Design 206 (2021) 109746.
[23] X. Ren, L. Xiao, Z. Hao, Multi-property cellular material design approach based on the mechanical behaviour analysis of the reinforced lattice structure, Materials & Design 174 (2019) 107785.
[24] M. Zhao, F. Liu, G. Fu, D.Z. Zhang, T. Zhang, H. Zhou, Improved Mechanical Properties and Energy Absorption of BCC Lattice Structures with Triply Periodic Minimal Surfaces Fabricated by SLM, Materials (Basel) 11(12) (2018).
[25] T. Tancogne-Dejean, D. Mohr, Stiffness and specific energy absorption of additively-manufactured metallic BCC metamaterials composed of tapered beams, International Journal of Mechanical Sciences 141 (2018) 101-116.
[26] X. Liu, T. Wada, A. Suzuki, N. Takata, M. Kobashi, M. Kato, Understanding and suppressing shear band formation in strut-based lattice structures manufactured by laser powder bed fusion, Materials & Design 199 (2021) 109416.
[27] L. Bai, C. Yi, X. Chen, Y. Sun, J. Zhang, Effective Design of the Graded Strut of BCC Lattice Structure for Improving Mechanical Properties, Materials (Basel) 12(13) (2019).
[28] L. Bai, Y. Xu, X. Chen, L. Xin, J. Zhang, K. Li, Y. Sun, Improved mechanical properties and energy absorption of Ti6Al4V laser powder bed fusion lattice structures using curving lattice struts,

Materials & Design 211 (2021) 110140.
[29] X. Chen, W. Ren, Y. Sun, J. Zhang, J. Yang, K. Wang, Y. Gong, Z. Zhang, L. Bai, Adjusting unit cell three-dimensional posture and mirror array: A novel lattice structure design approach, Materials & Design 221 (2022) 110852.
[30] M. Smith, Z. Guan, W.J. Cantwell, Finite element modelling of the compressive response of lattice structures manufactured using the selective laser melting technique, International Journal of Mechanical Sciences 67 (2013) 28-41.
[31] W.A. Chapkin, D.L. Simone, G.J. Frank, J.W. Baur, Mechanical behavior and energy dissipation of infilled, composite Ti-6Al-4V trusses, Materials & Design 203 (2021) 109602.
[32] X. Li, M. Kim, W. Zhai, Ceramic microlattice and epoxy interpenetrating phase composites with simultaneous high specific strength and specific energy absorption, Materials & Design 223 (2022) 111206.
[33] M. Leary, M. Mazur, J. Elambasseril, M. McMillan, T. Chirent, Y. Sun, M. Qian, M. Easton, M. Brandt, Selective laser melting (SLM) of AlSi12Mg lattice structures, Materials & Design 98 (2016) 344-357.
[34] S.H. Siddique, P.J. Hazell, H. Wang, J.P. Escobedo, A.A.H. Ameri, Lessons from nature: 3D printed bio-inspired porous structures for impact energy absorption – A review, Additive Manufacturing 58 (2022) 103051.
[35] X. Li, X. Yu, M. Zhao, Z. Li, Z. Wang, W. Zhai, Multi‐Level Bioinspired Microlattice with Broadband Sound‐Absorption Capabilities and Deformation‐Tolerant Compressive Response, Advanced Functional Materials (2022) 2210160.
[36] M.S. Pham, C. Liu, I. Todd, J. Lertthanasarn, Damage-tolerant architected materials inspired by crystal microstructure, Nature 565(7739) (2019) 305-311.
[37] C. Liu, J. Lertthanasarn, M.S. Pham, The origin of the boundary strengthening in polycrystal-inspired architected materials, Nat Commun 12(1) (2021) 4600.
[38] A. Kumar, L. Collini, A. Daurel, J.-Y. Jeng, Design and additive manufacturing of closed cells from supportless lattice structure, Additive Manufacturing 33 (2020) 101168.
[39] J. Yang, D. Gu, K. Lin, C. Ma, R. Wang, H. Zhang, M. Guo, Laser 3D printed bio-inspired impact resistant structure: failure mechanism under compressive loading, Virtual and Physical Prototyping 15(1) (2019) 75-86.
[40] J. Yang, D. Gu, K. Lin, Y. Yang, C. Ma, Optimization of bio-inspired bi-directionally corrugated panel impact-resistance structures: Numerical simulation and selective laser melting process, J Mech Behav Biomed Mater 91 (2019) 59-67.
[41] H. Jiang, L. Le Barbenchon, B.A. Bednarcyk, F. Scarpa, Y. Chen, Bioinspired multilayered cellular composites with enhanced energy absorption and shape recovery, Additive Manufacturing 36 (2020) 101430.
[42] Y. Wei, Q. Yang, X. Liu, R. Tao, Multi-bionic mechanical metamaterials: A composite of FCC lattice and bone structures, International Journal of Mechanical Sciences 213 (2022) 106857.
[43] Z. Li, C. Chen, R. Mi, W. Gan, J. Dai, M. Jiao, H. Xie, Y. Yao, S. Xiao, L. Hu, A Strong, Tough, and Scalable Structural Material from Fast-Growing Bamboo, Adv Mater 32(10) (2020) e1906308.
[44] R. Nishiyama, M. Sato, Structural rationalities of tapered hollow cylindrical beams and their use in Japanese traditional bamboo fishing rods, Sci Rep 12(1) (2022) 2448.
[45] M. Zou, S. Xu, C. Wei, H. Wang, Z. Liu, A bionic method for the crashworthiness design of thin-walled structures inspired by bamboo, Thin-Walled Structures 101 (2016) 222-230.

[46] D. Hu, Y. Wang, B. Song, L. Dang, Z. Zhang, Energy-absorption characteristics of a bionic honeycomb tubular nested structure inspired by bamboo under axial crushing, Composites Part B: Engineering 162 (2019) 21-32.
[47] Z. Zhang, L. Zhang, B. Song, Y. Yao, Y. Shi, Bamboo-inspired, simulation-guided design and 3D printing of light-weight and high-strength mechanical metamaterials, Applied Materials Today 26 (2022) 101268.
[48] T. Tancogne-Dejean, D. Mohr, Elastically-isotropic elementary cubic lattices composed of tailored hollow beams, Extreme Mechanics Letters 22 (2018) 13-18.
[49] M. Zhao, X. Li, D.Z. Zhang, W. Zhai, Design, mechanical properties and optimization of lattice structures with hollow prismatic struts, International Journal of Mechanical Sciences 238 (2023) 107842.
[50] M. Zhao, B. Ji, D.Z. Zhang, H. Li, H. Zhou, Design and mechanical performances of a novel functionally graded sheet-based lattice structure, Additive Manufacturing 52 (2022) 102676.
[51] D. Whitley, A genetic algorithm tutorial, Statistics and computing 4(2) (1994) 65-85.
[52] I. Maskery, A.O. Aremu, L. Parry, R.D. Wildman, C.J. Tuck, I.A. Ashcroft, Effective design and simulation of surface-based lattice structures featuring volume fraction and cell type grading, Materials & Design 155 (2018) 220-232.
[53] Z. Hashin, S. Shtrikman, A variational approach to the theory of the elastic behaviour of multiphase materials, Journal of the Mechanics and Physics of Solids 11(2) (1963) 127-140.
[54] J.B. Berger, H.N. Wadley, R.M. McMeeking, Mechanical metamaterials at the theoretical limit of isotropic elastic stiffness, Nature 543(7646) (2017) 533-537.
[55] P. Lohmuller, J. Favre, S. Kenzari, B. Piotrowski, L. Peltier, P. Laheurte, Architectural effect on 3D elastic properties and anisotropy of cubic lattice structures, Materials & Design 182 (2019) 108059.
[56] S. Altamimi, D.-W. Lee, I. Barsoum, R. Rowshan, I.M. Jasiuk, R.K. Abu Al-Rub, On Stiffness, Strength, Anisotropy, and Buckling of 30 Strut‐Based Lattices with Cubic Crystal Structures, Advanced Engineering Materials (2022) 2101379.
[57] Z. Chen, Y.M. Xie, X. Wu, Z. Wang, Q. Li, S. Zhou, On hybrid cellular materials based on triply periodic minimal surfaces with extreme mechanical properties, Materials & Design 183 (2019) 108109.
[58] J.J. Moré, The Levenberg-Marquardt algorithm: implementation and theory, Numerical analysis, Springer1978, pp. 105-116.
[59] I. Maskery, A. Hussey, A. Panesar, A. Aremu, C. Tuck, I. Ashcroft, R. Hague, An investigation into reinforced and functionally graded lattice structures, Journal of Cellular Plastics 53(2) (2016) 151-165.
[60] D.S.J. Al-Saedi, S.H. Masood, M. Faizan-Ur-Rab, A. Alomarah, P. Ponnusamy, Mechanical properties and energy absorption capability of functionally graded F2BCC lattice fabricated by SLM, Materials & Design 144 (2018) 32-44.
[61] L. Yang, C. Yan, C. Han, P. Chen, S. Yang, Y. Shi, Mechanical response of a triply periodic minimal surface cellular structures manufactured by selective laser melting, International Journal of Mechanical Sciences 148 (2018) 149-157.
[62] J. Kadkhodapour, H. Montazerian, A. Darabi, A.P. Anaraki, S.M. Ahmadi, A.A. Zadpoor, S. Schmauder, Failure mechanisms of additively manufactured porous biomaterials: Effects of porosity and type of unit cell, J Mech Behav Biomed Mater 50 (2015) 180-91.